ACIPET

Experimental and Theoretical Study of the Influence of Solvent on Asphaltene-Aggregates Thermo-oxidation through High-Pressure Thermogravimetric Analysis

O.E. Medina, Universidad Nacional de Colombia; I.M. Riascos, Ecopetrol S.A.; A.F. Pérez-Cadenas, Universidad de Granada; F. Carrasco-Marín, Universidad de Granada; C.A. Franco, Universidad Nacional de Colombia; and F.B. Cortes, Universidad Nacional de Colombia.

Categoría: Marque con una "X"

- Artículo Técnico [X]
- Tesis Pregrado [ ]
- Tesis Posgrado [ ]

Abstract

This study is focused on the understanding of *n*-C_7 asphaltene-aggregates oxidative behavior at high-pressure conditions. For this aim, different asphaltene model solutions were prepared using different solvents with similar solubility parameters but with different chemical structures, including *p*-xylene, *m*-xylene, and *o*-xylene, to evaluate the location of a methyl group of the solvent molecule on asphaltene aggregate size, solution viscosity and thermo-oxidation reactions. Small-angle X-ray scattering (SAXS) measurements were performed to estimate the aggregate size in different solvents, and rheological measurements were evaluated for varying concentrations of asphaltene between 0.1 and 10 % in mass fraction. For both low and high asphaltene concentrations, the viscosity (μ_r) and the asphaltene aggregate size increase in the order *o*-xylene < *m*-xylene < *p*-xylene. Also, molecular dynamics (MD) simulations were carried out to explain the aggregation differences, representing the asphaltenes as an average molecular structure dissolved in each xylene isomers. Radial distribution function (RDF), interaction energies, and aggregates size analysis were calculated. For this aim, it was found that the -CH_3 location in the xylene has a substantial impact on the aggregation and the viscosity. The MD results indicate that the *o*-xylene molecules surrounding the asphaltene aggregates oriented their -CH_3 groups towards the aggregates, increasing their interaction energy and reducing the aggregation size. Thus, a strong entropic volume effect was determined as a driving force due to the location of -CH_3, which has a strong impact on aggregation and rheological behavior. Further, high-pressure thermogravimetric analyses were performed to assess the thermo-oxidative behavior of asphaltene aggregates. In the first set of thermogravimetric experiments, the concentration of asphaltenes varied between 0.1% and 10% in mass fraction to evaluate its effect on the reactivity of the model solutions, using *p*-xylene as a reference solvent. The results showed that the oxygen chemisorption decreased as the asphaltene concentration increased in the system, and therefore, the reactivity was reduced. For a concentration of 0.1% by a mass fraction, there is no significant change in the thermogravimetric profiles in the different solvents used. However, with increasing the concentration to 1.0 and 10.0%, the mass gained by oxygen chemisorption increased in the order: *p*-xylene < *m*-xylene < *o*-xylene. This result indicates that the larger the size of the asphaltene aggregate, the lower the interactions with O_2, because of a reduction in active sites of the asphaltene structure due to the reduction in the surface area.

Keywords: Asphaltene aggregates, high-pressure, oxidation kinetics, thermo-oxidation reactions, solvents.

Introduction

Extra-heavy (EHO) and heavy crude oil (HO) are commonly subjected to thermal treatments from production to refining operations, involving asphaltene conversion under a wide range of operating conditions of pressure and temperature. Depending on the crude oil chemical nature, asphaltenes present different aggregation states that could affect the rheological behavior and subsequent thermal conversion.[1-3].[4] Thus, the study of the asphaltene fraction and aggregates is relevant to understanding their rheological properties and determining the best upgrading scheme for HO and EHO during thermal treatments.[5, 6]

Most of the studies[7-10] have been focused on evaluating the thermo-oxidative behavior of asphaltene molecules at low and high pressure. The found thermograms suggested that the asphaltene thermal oxidation is pressure-dependent and occurs in four mainly thermal events,

namely *i*) oxygen chemisorption (OC), *ii*) oxygen decomposition of chemisorbed oxygen functional groups (DCO), *iii*) the first combustion (FC), and *iv*) second combustion (SC) or high-temperature oxidation, for pressures higher than 0.7 MPa.[9] The OC and DCO disappear for pressures < 0.7 MPa.

Nevertheless, asphaltenes have high polarity and complex structure; they present a high self-association degree during heavy oil processing. Thus, further efforts are needed to provide more comprehensive knowledge and understand the processes of asphaltene decomposition, considering the complexity of the aggregation state of asphaltenes in the crude oil matrix.

Molecular dynamics (MD) simulations have become a valuable tool in that regard. Some authors have used representative asphaltene model solutions to study variables such as viscosity and asphaltene aggregate size, among others.[11 12 13, 14] Moncayo et al.[11] studied the methyl substituent (-CH_3) effect on the rheological behavior of model solutions of asphaltenes at different concentrations, comparing *p*-xylene and toluene. In addition, MD simulations evidence that solvent characteristics strongly influence asphaltene aggregation.[15-17] They determined an increase in the viscosity as the asphaltene concentration increases, 739 % higher in *p*-xylene than toluene. Also, Larichev et al.[14] evaluated the influence of various organic compounds on the aggregation of asphaltenes, obtaining a higher length of 13.6 nm for a consisting solution of 20 % in mass fraction of asphaltene diluted on furfural. In this current context, solvents can affect the aggregation phenomenon and rheologic behavior of asphaltene model solutions. However, the relationship between asphaltene aggregation state and rheologic behavior has not been studied or reported in the literature. Furthermore, solvents might differ in their maximum oxygen solubility, which might impact the oxygen transfer reaction of asphaltenes, affecting their reactivity.[18] Indeed, depending on the identity of the solvent, several mechanistic routes are possible, including hydrogen abstraction from the solvent and radical accepting capability.[11]

Regarding the mechanism, several factors influence the aggregates interactions, including thermo-oxidation of labile bonds, asphaltene structure, asphaltene condensation degree, and thus, the aggregate structure.[10]

Hence, this work aims to understand for the first time the thermo-oxidative behavior at high pressure of different asphaltene model solutions varying states of aggregation. This study includes the effect of other solvents, including *o*-, *m*-, and *p*-xylene, on asphaltene-aggregate size and viscosity of asphaltene model solutions. The analysis was done experimentally through SAXS and rheological measurements and theoretically using molecular dynamic simulation. Then the reactivity was analyzed by high-pressure thermogravimetric experiments. In the first set of thermogravimetric experiments, the effect on the reactivity of the concentration of asphaltenes varied between 0.1% and 10% in a mass fraction was evaluated, using *p*-xylene as a reference solvent. Then, three aromatic solvents (*p*-xylene, *m*-xylene, and *o*-xylene) have similar solubility parameters but different chemical structures. This is the first work that addressed the effect of aggregation state on asphaltene reactivity at high-pressure conditions. It is hoped that a new landscape can be open to deepening knowledge and understanding of thermo-oxidation reactions of asphaltene aggregates.

Experimental.

Materials. A Colombian extra-heavy crude oil was employed for *n*-C_7 asphaltene isolation following the ASTM standard.[19] The crude oil has 6.7 ° API, a viscosity of 6×10^6 cP at 25 °C, and SARA content of 13.0, 16.9, 49.9, and 20.2% $w \cdot w^{-1}$, respectively. *n*-heptane (99.5%, Sigma-Aldrich, St. Louis, MO, USA) was used for asphaltene extraction. The chemical and physical properties are summarized in detail in a previous study.[20]

For the thermogravimetric analyses, the reacting gas employed consists of synthetic air NTC 2561 (CRYOGAS, Bogotá, Colombia) composed of 20.93% balanced O_2. *p*-Xylene, *m*-xylene, and *o*-xylene (98%) were purchased from ITW Reagents (Chicago, USA). The basic properties of the selected diluents provided by the supplier are summarized in Table 1.

Table 1. General properties of the diluents used for preparing asphaltene model solutions.

Diluent	Density ($mg \cdot L^{-1}$)[a]	Viscosity (cp)[a]	Molecular weight ($g \cdot mol^{-1}$)	Purity (%)	Solubility parameter δ ($\gamma \cdot V^{-1/3}$ $dyn \cdot mol^{1/3} \cdot cm^{-2}$)
p-xylene	0.864	0.644	106.17	98.0	5.7
m-xylene	0.860	0.617	106.17	98.0	5.8
o-xylene	0.880	0.809	106.17	98.0	6.1

[a]Measured at 25 °C.

Solution model preparation. *n*-C_7 Asphaltene model solutions were prepared by slowly adding the asphaltenes to the respective diluents while the mixture was magnetically stirred at 300 rpm for 30 min. Different model solution consisting of mass fractions of 0.1 %, 1.0 %, and 10.0 % of *n*-C_7 asphaltenes were prepared. The total dilution of the samples was confirmed by optical microscopy.

Aggregate size measurements. Asphaltene aggregate sizes on the different solvents were registered by Small-angle X-ray scattering (SAXS) using an S3-MICRO diffractometer (Hecus, Austria) with a Cu anode ($\lambda_{CuK\alpha}$= 1.541 Å). The patterns were analyzed in the wave factor range (h) between 0.01 and 0.6 $Å^{-1}$, which is defined by the expression (1):

$$h = 4\pi \sin(\theta) / \lambda \quad (1)$$

where 2θ are the scattering angle and λ the wavelength of the applied radiation using 1.5 mm quartz capillaries. The patterns for asphaltenes were obtained by subtracting the corresponding SAXS of the initial solvents to the asphaltene solutions, considering the X-ray absorption coefficients.[18, 21]

The radius of gyration (R_G) of the particles was assessed by the slope of the small-angle curve of the graph ($ln(I(h))$ against h^2), whereas the radius of gyration of the cross-section ($R_{G(cross)}$) of the particles was obtained by the slope of the plot ($ln(I(h)) \times h$ against h^2) as long as $R_G \times h < 1.3$.[22, 23]

Finally, the fitting of the SAXS results was analyzed via the ellipsoid model (Equation (2)):

$$I(h) = \int_0^\infty F(h,R) \times D_v(R) dR \quad (2)$$

where $F(h,R)$ is an average form factor and $D_v(R)$ is the volume size distribution of the dispersed particles. Considering that HP-TGA measurements were performed after flash solvent evaporation, the aggregate size of the asphaltenes after the process was estimated to corroborate that the size of the asphaltene aggregate is not affected during flash evaporation of the solvent. Flash evaporation was carried out at the evaporation temperature of each solvent using a rotary evaporator with a speed of 70 rpm for 5 min. Data were processed in the ATSAS program package (version 2.4).[24]

Viscosity determination. The viscosity of the *n*-C_7 asphaltene solutions was determined by rheological measurements using a Kinexus Pro rotational rheometer (Malvern Instruments, Worcestershire – UK) at 25 °C in a shear rate range between 1 and 100 s^{-1}. For samples with mass fractions of 0.1% and 1.0% of *n*-C_7 asphaltenes, concentric cylinders geometry was employed, whereas for solutions with 10.0%, a 20 mm plate-plate geometry was with a gap of 0.3 mm. Also, results are reported as relative viscosities ($\mu_r = \mu_{solution} / \mu_{solvent}$), i.e., the viscosity of the *n*-C_7 asphaltene ($\mu_{solution}$) solution divided by the solvent's viscosity ($\mu_{solvent}$). Measurements were done by triplicate to ensure repeatability.

High-Pressure Thermogravimetric Analysis. High-pressure thermogravimetric analyzer HP-TGA 750 (TA instruments Inc., Hüllhorst, Germany) containing a magnetically levitated balance was employed to appraise the thermal behavior of different *n*-C_7 asphaltenes under an air atmosphere at high pressure (6.0 MPa). Details of the system equipment are reported elsewhere.[25] Flash evaporation was realized before TGA measurements to avoid diffusional effects on thermal profiles so that the impact of the state of aggregation of asphaltene is achieved. The tests were carried out using a heating ramp of 10 °C·min^{-1} from 100 °C to 800 °C under an airflow of 80 mL·min^{-1}. The pressure was maintained at 6.0 MPa, while the sample mass was set at 1 mg after flash solvent evaporation to avoid diffusional effects of mass and heat transfer, according to the results obtained in a previous study.[26] The evaporation process was done at the boiling point of the respective solvent used and at vacuum pressure to ensure that the asphaltenes did not oxidize.
Each test was performed by triplicate to ensure repeatability of the results, obtaining a ± 0.01 °C uncertainty.

Molecular dynamics methods. To obtain some physical insights into the effect of the methyl group (-CH_3) location on the aggregation behavior in xylene isomers, molecular dynamics (MD) simulations were carried out. For this, asphaltenes were represented by a single average structure dissolved in each xylene isomer (ortho, meta, and para). The theoretical evaluation was carried out for the concentration of 10% in the asphaltene fraction. To this aim, 27 molecules were used to represent the experimental model solutions computationally since this number allows obtaining a reliable representation of the state of aggregation according to results reported in the literature and previous studies.[11, 27, 28] Then, the number of xylene molecules necessaries was calculated to represent an asphaltene concentration of 10 %, i.e., 2086 molecules of xylene were employed. Asphaltene and solvents were simulated using the optimized potential for liquid simulations (OPLS),[29, 30] widely used to describe organic compounds such as crude oil and asphaltenes. Lennard-Jones (12-6) and Coulombic models were used to describe intermolecular interactions, van der Waals type, and electrostatic, respectively. In the case of bonds and angles flexions, they were represented by harmonic models, whereas the model proposed by Watkins and Jorgensen [31] was used to describe the torsions.

To obtain an adequate explanation of the aggregation behavior of asphaltenes, the three stages were carried out, used to study the aggregation of asphaltenes in a previous study,[11] satisfactorily describing the experimental measurements. First, the initial configuration was simulated in an NVT (i.e., at volume, temperature, and number of molecules constant) ensemble was used at 400 K and an initial density of 0.4 g·cm^{-3} (simulation box expanded), during 0.5 ns with a time step of 1 fs. Then, at the same density, other 1.5 ns were conducted using an NVT ensemble at 298 K. This first stage was carried out to guarantee that the initial configuration corresponds to minimum energy, preventing it from dropping into a local minimum. In the second stage, the density of equilibrium was determined. An NPT (i.e., pressure, temperature, and number of molecules constant) ensemble was used during 3 ns at 298 K and 1 atm. Finally, after the equilibrium density was reached in the third stage, an NVT ensemble was conducted to fully equilibrate the system during 25 ns of simulations with a time step of 2 fs. Hence, 30 ns were simulated for each asphaltene solution. In addition, periodic boundaries were considered in all directions.
To evaluate the effect of the -CH_3 location on the aggregation behavior, radial distribution function (RDF), asphaltene-asphaltene interaction energies, and root mean square displacement (RMDS) calculations were carried out. A detailed description of how these calculations were carried out can be found elsewhere.
MD simulations were performed using LAMMPS.[32] In addition, VMD [33] was used to visualize the simulations, obtain images, and calculate the radial distribution function. The Nosé-Hoover thermostat and barostat were used to fix the temperature and pressure, respectively. The cross-interaction parameters between atoms of different species were determined using geometric mixing rules. The cutoff radius was set at 16 Å for both van der Waals and electrostatic interactions. Whereas long-range electrostatic interactions were calculated using the particle-particle-particle mesh method.

Kinetic analysis of asphaltene oxidation

Thermal behaviour analysis is performed to obtain information about the kinetic parameters of thermo-oxidation of asphaltene aggregates at high-pressure conditions in different temperature regions. [34, 35] Effective activation energy is calculated using the slope of the $\ln\left[\frac{\beta(-\ln(1-x))}{\mathrm{P}_{O_2}^{n}T^{2}}\right]$ against $\frac{1}{RT}$ obtained from Equation 3. Details of the kinetic model are shown in several works.

$$\ln\left[\frac{\beta(-\ln(1-x))}{\mathrm{P}_{O_2}^{n}T^{2}}\right]=\ln\left(\frac{k_o R}{E_a}\right)-\frac{E_a}{RT} \qquad (6)$$

where $\mathrm{P}_{O_2}^{n}$ (bar) represents the partial pressure of the reactant gas (O_2), n the order of reaction, R (J×mol^{-1}K^{-1}) the universal gas constant, E_a (kJ×mol^{-1}) the effective activation energy, k_o (s^{-1}×bar^{-n}) the pre-exponential factor. The volumetric model for a radial consumption of the *n*-C_7 asphaltenes is represented in the expression $f(\theta)=(1-\theta)$ [36].

Results.

Asphaltene Characterization. Briefly, carbon, hydrogen, oxygen, sulfur, and nitrogen content were 81.7, 7.8, 3.6, 6.6, and < 0.5 % in mass fraction, respectively. The molecular weight M_{W} of *n*-C_7 asphaltenes was 907.3 g·mol^{-1}. Using X-ray diffraction (XRD) it was obtained the inter-aromatic layer distance (d_m), and inter-chain or inter-naphthenic layer distance (d_γ) in *n*-C_7 asphaltenes were 3.47 Å and 5.61 Å, respectively. The average height of the stacked aromatic sheets perpendicular to the sheet plane (L_c) was found at 13.93 Å, and the average diameter of the aromatic sheet (L_a) was equal to 19.06 Å. Finally, according to M value, there are approximately 5 aromatic sheets in the stacked cluster. The results are similar to the reported for asphaltenes isolated from EHO.[10, 37] From ^{1}H-NMR was obtained the proportional distribution relationship of aromatic hydrogen (H_a), aliphatic hydrogens α, β, and γ linked to aromatic rings, named H_α, H_β, and H_γ, respectively. Results show a relative amount of H_α of 23.49%, attributed to the high aromaticity degree reported by bulk tests. Aliphatic hydrogen follows the order: H_α (4.79%) < H_γ (8.98) < H_β (62.72%). Through the ^{13}C-NMR analysis, the total content of 35.51% for aliphatic carbon (C_{al}) and 64.48% for aromatic carbon (C_{ar}) as was identified, which agrees with the reported in the literature.[10, 38, 39] Through the modified Brown-Ladner method, [40] average structural parameters (APS) were quantified using results from ^{1}H-NMR, elemental analysis, and vapor pressure osmometry. Table 1 of Appendix A summarizes the results obtained.
The average molecular structure for the asphaltene studied was reported in a previous study, [20] with a proposed molecular formula of $C_{62}H_{70}S_2O_2$..

Asphaltene aggregates characterization. Experimental results of SAXS and rheological measurements are presented in this section. Figure 1 shows the results from a) SAXS and b) experimental relative viscosity (μ_r) for different asphaltene concentrations dissolved in

p-, *m*-, and *o*- xylene. Similar trends were found for asphaltene aggregate size and relative viscosity for solution models. As the asphaltene concentration in the model solution increases, the asphaltene aggregate size and the viscosity rise. Therefore, as the asphaltene aggregate size increases, the viscosity of the solution model is increased too, which agrees with the trends reported in the literature.[11, 41] These results are associated with the overlapping ability of asphaltenes, which increases the elasticity of the fluid.[42] Furthermore, viscosity is also affected by the diluent used. For both low and high asphaltene concentrations, μ_r increases in the order *o*-xylene < *m*-xylene < *p*-xylene, indicating that the position of a methyl group affects the asphaltene size and viscosity of the model solution prepared. Some differences were found in both variables as the concentration of the asphaltene changed. In the first instance, for a mass fraction of 0.1% of asphaltenes, the relative viscosity for all solutions was similar between 3 and 5 a.u. When asphaltene concentration increased up to 1.0% in mass fraction, viscosities vary from 69 a.u. (*o*-xylene) to 89 a.u. (*p*-xylene), correlated with a higher variation in asphaltene aggregate size (8.19 nm to 8.99 nm). For the systems with 10.0% in mass fraction of asphaltenes, the viscosity varies by more than 1700 u.a. between the system with the lowest viscosity (*o*-xylene) and the system with the highest viscosity (*p*-xylene). In particular, the aggregate size in systems at the concentration of 10.0% by mass fraction varies to a greater extent. This behavior is closely related to the asphaltene aggregate sizes, promoted by the heteroatom content (N, O, and S) in the chemical structure and the self-association behavior of asphaltenes.[43] The aggregation mechanisms gain importance at high concentrations, increasing the interactions between the aromatic cores forming aggregates by full stacking.[11] Hence, the results indicate that the asphaltene solution models behave as concentrated suspensions, considering that an increase in volumetric fraction promotes an increase in viscosity.[11]
It is expected that its state of aggregation strongly influences the interaction energies between asphaltenes molecules. This evidence that the position of the -CH_3 substituent in the xylene structure can modify the fluid's internal network from a volume entropic effect, as shown later in MD results.[11, 41]

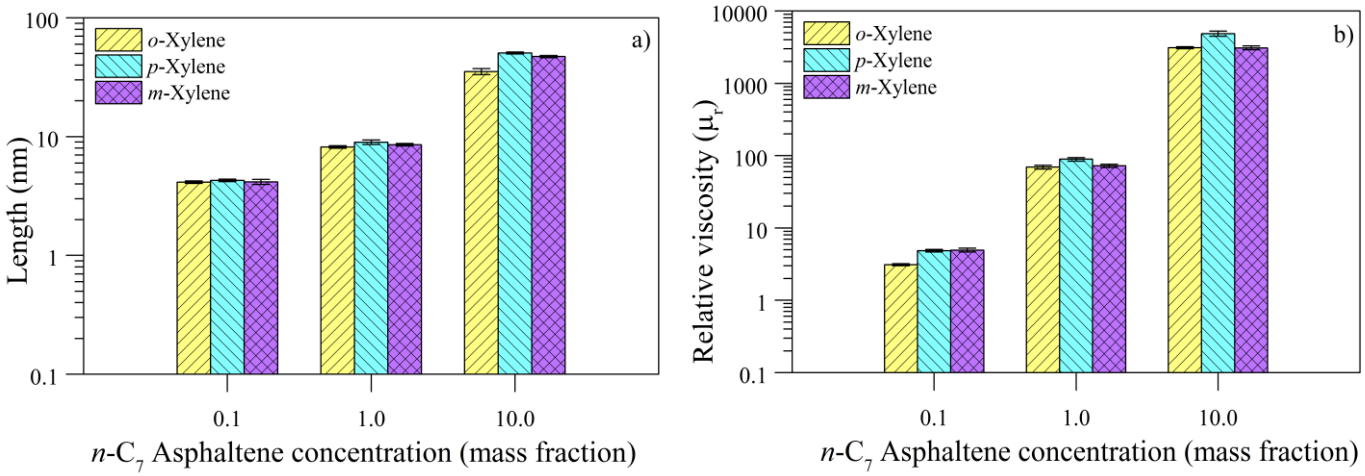

Figure 1. Average length (L) of *n*-C_7 asphaltenes particles in different organic solvents and b) relative viscosity ($\mu_r=\mu_{solution}/\mu_{solvent}$), for asphaltene solution in different aromatic solvents. The viscosity was taken for a shear rate of 10 s^{-1}.

Molecular dynamic simulation. MD simulations were carried out to estimate the effect of the –CH_3 location on the aggregation behavior. To this aim, RDF, the average size of asphaltene aggregates, asphaltene-asphaltene, and asphaltene-xylene interaction energies, and the root mean square displacement (RMDS) were calculated. Figure 2 shows the final configuration of the asphaltenes after the system was fully equilibrated. Figure S1 of the supplementary material shows the RMSD results, indicating that the time simulations conducted were enough to guarantee that the aggregation state converged to an equilibrium state.[11, 44]

a.

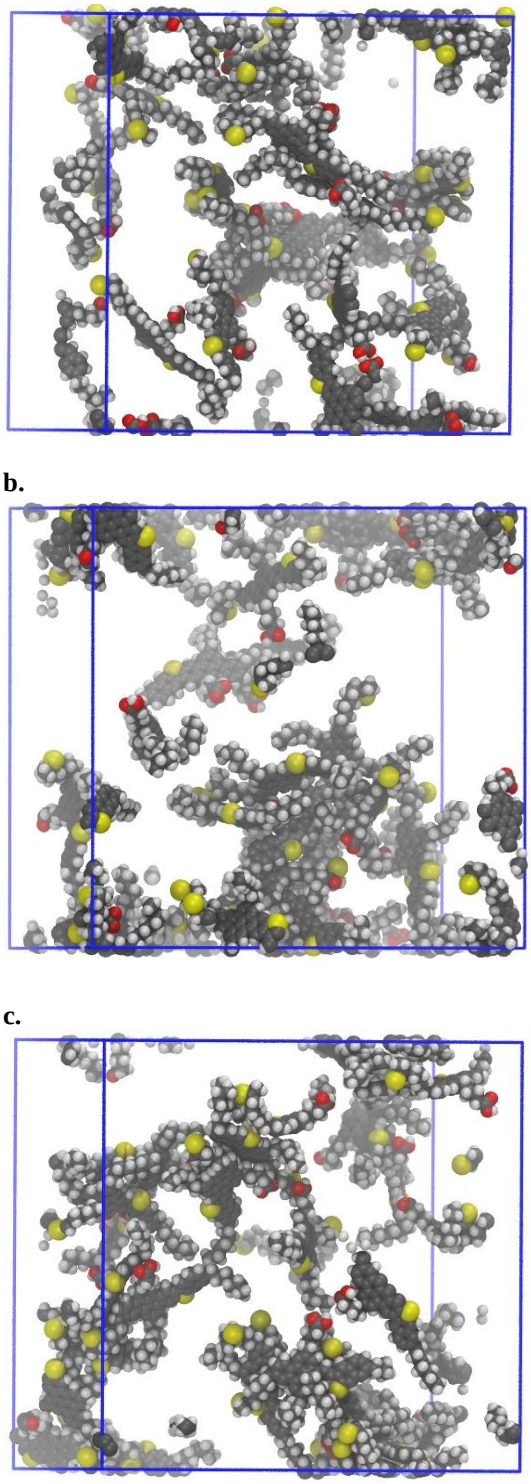

Figure 2. Asphaltenes aggregates at the final configuration at an asphaltene concentration of 10 % in mass fraction dissolved in (a) *o*-xylene, (b) *m*-xylene, and (c) *p*-xylene. For clarity, solvent molecules are hidden. Carbon atoms are shown in gray, hydrogen in white, sulfur in yellow, and oxygen in red.

Figure 3 shows the RDF results between the center of mass of the asphaltenes molecules in each solution evaluated in MD simulations, at an asphaltene concentration of 10 % in mass fraction. The results indicate significant differences in the internal structure of each asphaltene solution. The RDF curve of the asphaltenes dissolved in *p*-xylene evidence the highest coordination peak at 6.35 Å, whereas the RDF curves for *m*-xylene and *o*-xylene are displaced to the right at 7.05 Å and 7.35 Å, respectively. This result suggests that the

aggregation behavior is altered due to the location of the methyl substituent in the xylene molecular structure. To corroborate this, the average of the asphaltene aggregate size was calculated.

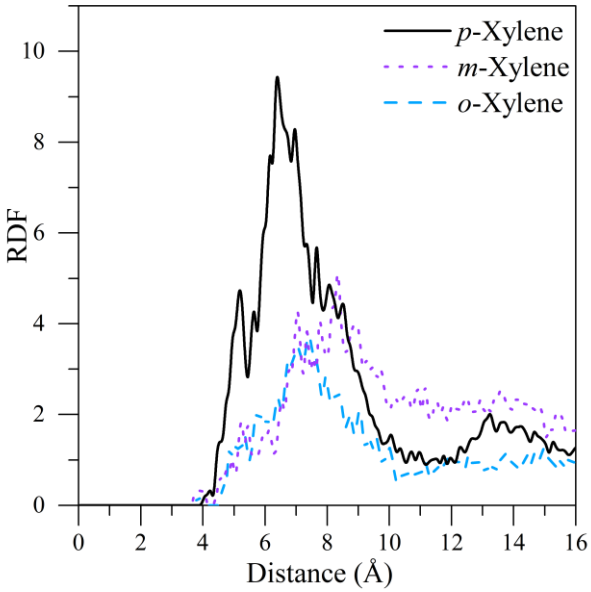

Figure 3. Radial distribution function (RDF) between the center of mass of the asphaltene molecules dissolved in each solvent at a concentration of 10% in mass fraction.

Figure 4 shows the average size of the asphaltene aggregates, corroborating that the aggregation behavior is affected by the location of the methyl in the xylene molecular structure. The results indicate that the state of lowest aggregation corresponds to asphaltenes dissolved in *o*-xylene, followed by *m*-xylene and *p*-xylene, in that order. An increase of 6% is obtained in the average size of aggregates, comparing *m*-xylene with *o*-xylene, and an increase of 23% concerning *p*-xylene. In all cases, the size of the aggregate does not exceed 2.1 molecules per aggregate. This value is significantly higher when compared with the data reported in the literature. Headen et al.[28] obtained aggregate sizes of 4.35 molecules per aggregate, evaluated in toluene at an asphaltene concentration of 7%. At the same asphaltene concentration, an average size of 4.5 molecules per aggregate was obtained in previous work. Considering that the aggregation increases as the concentration of asphaltenes increases,[11] these results indicate that xylene isomers can dissolve asphaltenes than toluene, the most widely used solvent in asphaltene solution models.

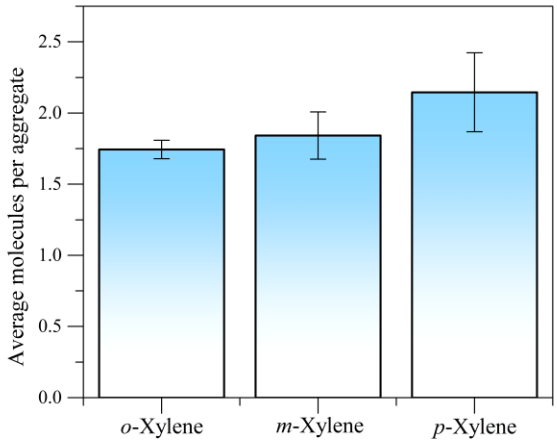

Figure 4. Average size of asphaltene aggregates of each solution evaluated by MD simulations at an asphaltene concentration of 10 % in mass fraction.

Figure 5 shows the asphaltene-asphaltene and asphaltene-solvent interaction energies for each solution model evaluated by MD simulations. It is worthing to note that positive energies denote repulsion, whereas negative interaction energies denote attraction. As mentioned above, these calculations are carried out as an average over molecules pairwise considered. This means that it considers all contributions, and thus, despite Figure 5-a showing that asphaltene-asphaltene interaction energies denote repulsion, this does not imply that asphaltenes are not aggregated. Still, it indicates that, on average, the asphaltene trend to keep dispersed compared to the molecules aggregated. Previous work found that these asphaltene-asphaltene interaction energies are positive for low asphaltene concentrations, and it becomes negative as the asphaltene concentration increases.[11, 44] For toluene, it was found that the asphaltene-asphaltene interaction energy is -2.45 kcal×mol^{-1}, at an asphaltene concentration of 7 % in mass fraction, which is due to the difference of the aggregation state shown above. As higher is the aggregation state of the asphaltene, higher will be their interaction energy on average. On the other hand, the asphaltene-xylene interaction energies are negative, denoting attraction in all cases. A clear tendency can be observed comparing both interaction energy results. As more positive are the asphaltene-asphaltene interaction energies, more negative are the asphaltene-xylene interaction energies (*o*-xylene < *m*-xylene < *p*-xylene in that order). This behavior is directly correlated with the aggregation state of the asphaltenes in the solution. As the asphaltene molecules remain dispersed, they are surrounded by a determined number of xylene molecules (coordination number). Hence the surface area contact of an asphaltene with the solvent molecules is higher than asphaltene molecules aggregated. This indicates that *o*-xylene allows that asphaltenes remain more dispersed compared to the other two xylene isomers.

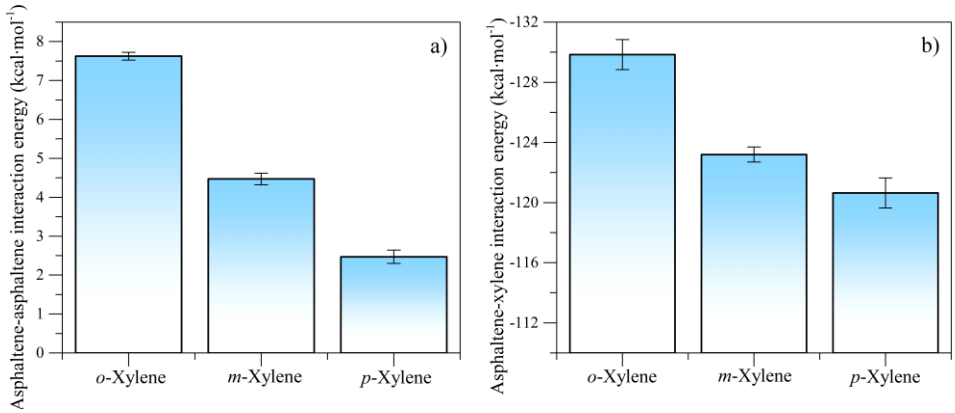

Figure 5. Average of the interaction energy between (a) the asphaltenes and (b) asphaltene-solvent pairwise.

Finally, the RDF between the center of mass of the asphaltene molecules and the carbon atoms of the methyl substituent of each xylene isomer were calculated to determine what structural changes are due to the location of the –CH_3. Figure 6 shows the results obtained indicating significant differences in the xylene molecules located around the asphaltene molecules. This showed that the methyl substituents are oriented towards asphaltenes, in the case of *o*-xylene, increasing the number of near and far neighbors compared to the other two cases.

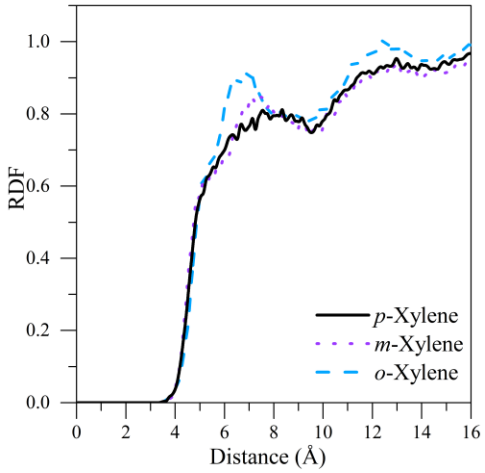

Figure 6. RDF between the center of mass of the asphaltene molecules and the carbon atoms of the methyl substituent of each xylene isomer.

Therefore, a strong entropic volume effect is observed due to the location of the -CH_3, which increases the asphaltene-xylene interaction energies impacting the aggregation behavior. Figure 7 shows how xylene molecules are distributed around two asphaltenes aggregated, located at 2.5 Å. This illustrates the results reported in Figure 6, indicating that the –CH_3 substituents are mainly oriented toward the asphaltene molecules, increasing their interaction energy and thus reducing the aggregation trend. For this reason, both experimentally and theoretically, it was found out that *o*-xylene reduces the aggregation compared to the other two xylene isomers.

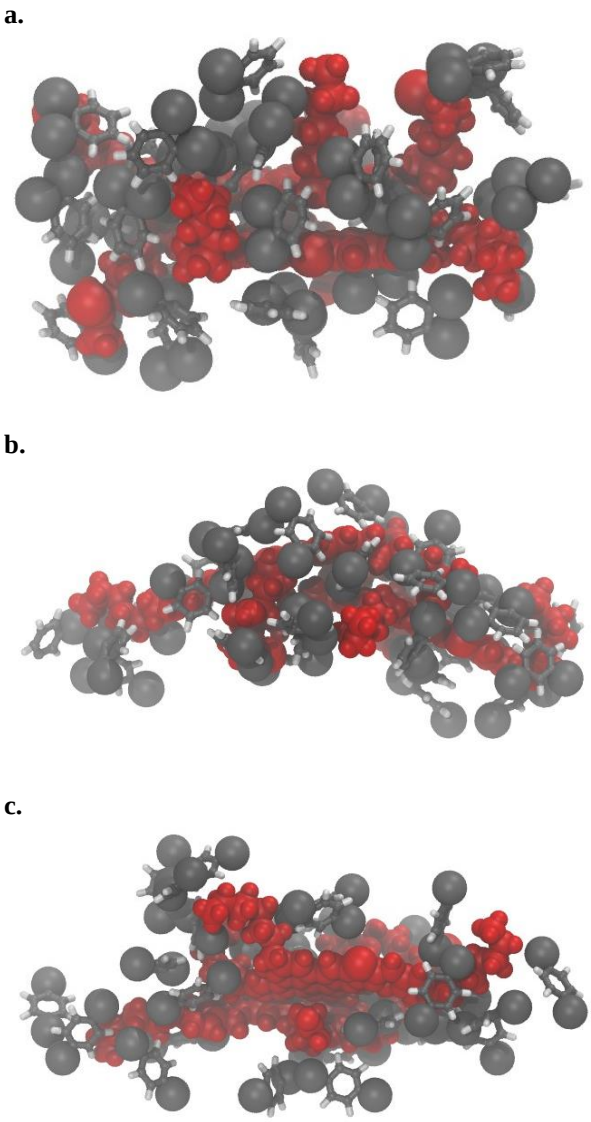

Figure 7. Asphaltene aggregate composed of two molecules surrounded by (a) *o*-xylene, (b) *m*-xylene, and (c) *p*-xylene. The whole asphaltene molecule is shown in red, carbon in gray, and hydrogen in white.

High-Pressure experiments. The thermo-oxidative reactivity of the different samples was evaluated in different steps, including *i*) the effect of the concentration of asphaltenes diluted in *p*-xylene as a reference solvent, and *ii*) the impact of the addition and position of a methyl group in the model solutions (*p*-, *m*-, and *o*-xylene) for different asphaltene concentrations.

Effect of n-C_7 asphaltene content. The effect of the *n*-C_7 asphaltene content was assessed by estimating the oxidation profiles at a fixed pressure (6.0 MPa) to different model solutions containing mass fractions of 0.1%, 1.0%, and 10.0% of asphaltenes diluted in *p*-xylene. Figure 8 a-b shows the mass change and rate for mass change profiles obtained, while the thermogravimetric characteristics are found in Table 2 of Appendix A. As a first instance, it is observed that regardless of the asphaltene concentration, when the

system is subjected to high pressure, the thermograms are described by the four thermal events *i*) oxygen chemisorption (OC), *ii*) oxygen decomposition of chemisorbed oxygen functional groups (DCO), *iii*) first combustion (FC), and *iv*) the second combustion.

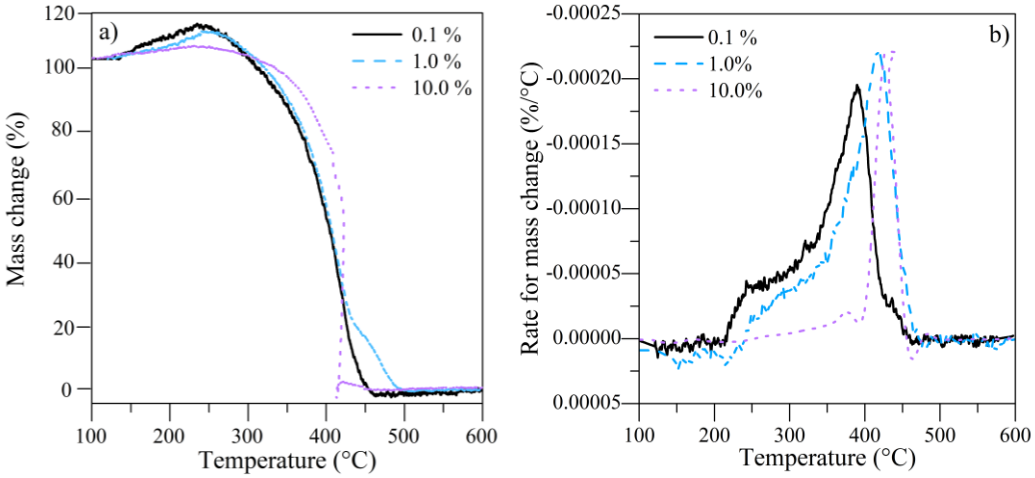

Figure 8. Mass percentage and rate for mass change for the thermo-oxidation of *n*-C_7 asphaltene model solutions in *p*-xylene for different asphaltene concentrations of 0.1% 1.0% and 10.0% at 6.0 MPa. Sample weight: 1 mg, heating rate: 10 °C·min^{-1}, and airflow: 80 mL·min^{-1}.

Interestingly, substantial differences were found in the different thermal stages as the asphaltene content increases in the model solutions. Notwithstanding, it is essential to mention that *p*-xylene is the solvent in which the size of the asphaltene aggregate was affected to a greater degree with the increase in asphaltene concentration than the rest of the aromatic solvents considered in this study.

The thermograms show that the amount of oxygen chemisorbed increases as the asphaltene concentration decreases, which is intrinsically attributed to the size and surface area of the aggregates and the subsequent thermal expansion. The results suggest that the smaller aggregates present a higher surface area/volume ratio. Therefore, they offer more active sites for interacting with O_2, representing a more representative adsorbed mass fraction than larger agglomerates. Furthermore, its thermal expansion occurs naturally, having immediate exposure to the gas phase. Moreover, by increasing the aggregate size, there is a reduction in the active sites for oxygen anchoring.[12, 45, 46] Aromatic structures are less exposed to oxidation. For example, pyridines, pyrroles, and thiophenes, which in previous works were shown to play a fundamental role in OC, would now be clogged in the aggregate complexes.[10] Other groups such as COO-, could also reduce their interaction with O_2 since they depend on the ionizing of carboxyl, which in turn, depends on the activation of -OH groups.[47] Scheme 1 shows a representative scheme for OC of different asphaltene aggregate sizes.

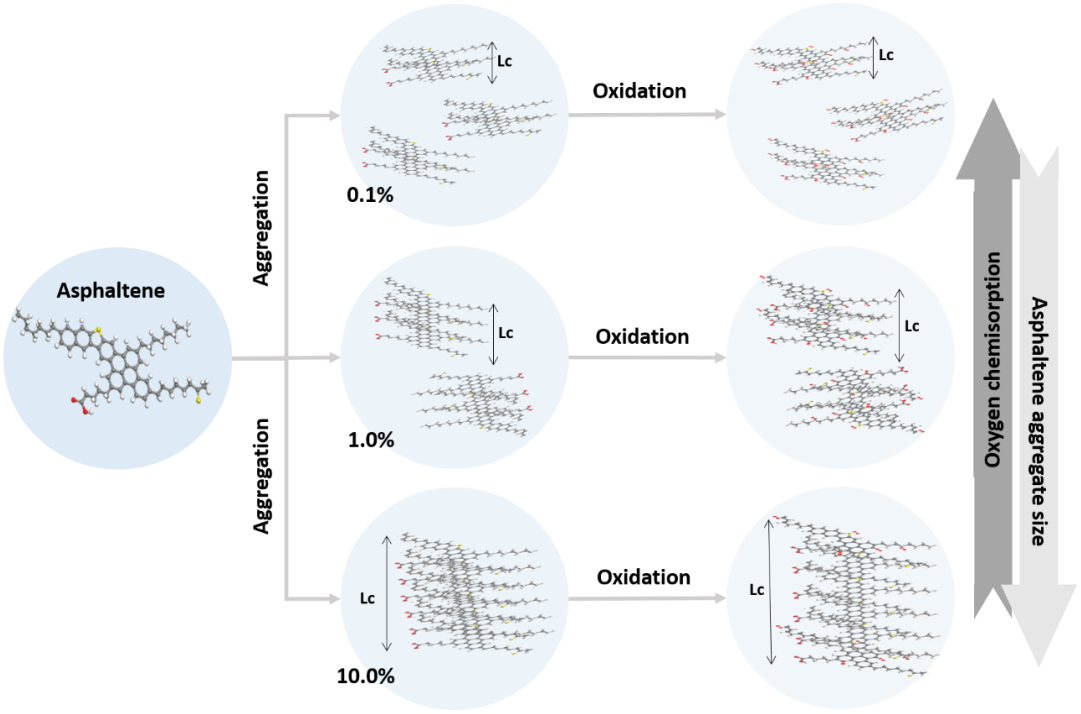

Scheme 1. Mechanistic representation of asphaltene aggregation considering π -stacking interactions at different concentrations (0.1%, 1.0%, and 10.0% in mass fraction) diluted in *p*-xylene and subsequent oxidation at high-pressure conditions.

DCO zone is also affected by the asphaltene aggregate state because subsequent thermal events depend on the structures created in OC. In this sense, the systems that formed structures with higher reactivity spread DCO at higher temperatures than those with low oxygen chemisorption. The system with 0.1% by the mass fraction of asphaltenes in *p*-xylene ends DCO at lower temperatures, further losing more mass than the systems with 1.0 and 10.0% by a mass fraction. In this context, combustion zones also show differences between each system. According to panel b of Figure 8, the system with 0.1% presents low intensities for FC and SC zones, whereas the systems with 1.0 and 10.0% present the opposite behavior. The trend is clearly observed; the intensity of the two last peak increases with increasing aggregate size (0.1% < 1.0% < 10.0%). It has been shown that the critical nanoaggregate concentration (CNC) of asphaltenes in *p*-xylene is between 0.1 - 3.4 $g \times L^{-1}$, which is similar to critical micelle concentration in surfactant solutions.[48] In this sense, it is evident that the systems with 1.0 and 10.0 % in mass fraction of asphaltenes are higher than CNC. Therefore, thermo-oxidative reactions require higher temperatures to produce complete oxidation of the organic matter. This is a consequence of the low reactivity that samples present due to the low OC and the more condensed structure resulting after DCO. The following Figure (Figure 9a-b) shows the change in oxygen chemisorption and length of the second combustion peak of the rate for mass change as a function of the viscosity and aggregate length. From panel a, the trend is clear. At a larger asphaltene aggregate size, chemisorption is reduced in response to the reduction in the area/volume ratio of the system. The active sites available for the anchoring of oxygen in the molecular structure of asphaltene are reduced when the aggregate is larger. Similarly, solutions with a higher degree of viscosity follow the same trend. The viscosity of the system is related to the size of aggregate formed in it. The systems with the highest viscosity were the systems with the largest aggregate size of asphaltenes. Also, the length of the SC peak increases as the aggregate size decreases. The width of a peak on a rate for mass change curve is a characteristic property in the decomposition of asphaltenes. As the width of the peak decreases, there is a greater distribution of the molecular weight of the molecules. In this case, the largest aggregates have a homogeneous molecular weight, and their decomposition takes place violently and at very high temperatures. In systems with the largest width, their decomposition is generated progressively from low temperatures for smaller aggregate sizes, as in 0.1 and 1.0% in mass fraction.

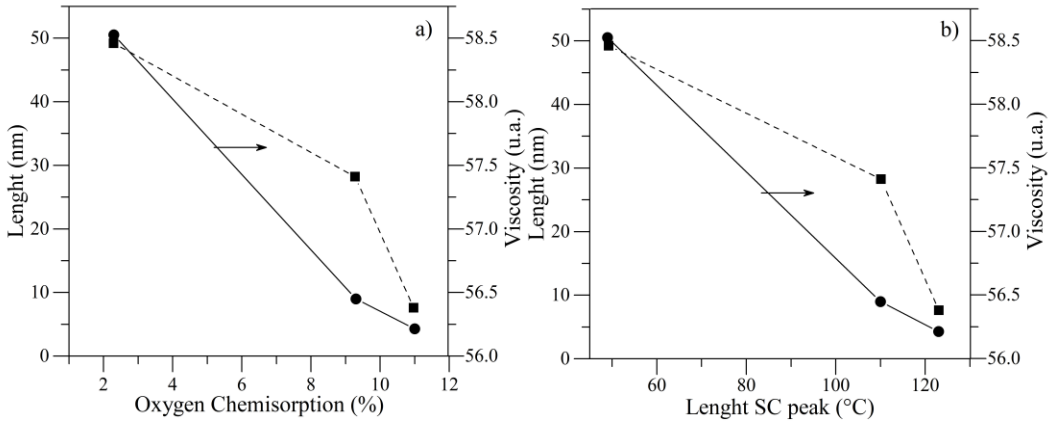

Figure 9. Relationship between asphaltene aggregate size and viscosity of the model solutions with a) oxygen chemisorption and b) length of the SC peak for systems with 0.1, 1.0, and 10.0 % in mass fraction of asphaltenes in *p*-xylene.

Effect methyl position. It has been shown that the addition of methyl groups and its position in the xylene molecule affect the asphaltene aggregate size and the viscosity of the system. Hence, this section is focused on studying their effect on oxidative reactivity at high-pressure conditions. The tests were done for three asphaltene concentrations (0.1, 1.0, and 10.0% in mass fraction). The results are shown in panels a-f of Figure 10, and thermogravimetric characteristics are shown in Table 3 of the Appendix A. The results indicate that the thermal profiles are influenced by both properties; notwithstanding, it also depends on the asphaltene concentration used. Panels a-b shows the mass change and rate for mass change for an asphaltene concentration of 0.1% in mass fraction, from which it is observed that the thermograms can be divided into four regions: OC, DCO, FC, and SC for all cases (*o*-xylene, *m*-xylene, and *p*-xylene). Each region ends at similar temperatures for this concentration, and the mass lost in DCO, FC, and SC does not differ significantly.

The differences in thermogravimetric profiles become more noticeable as the concentration of asphaltenes in the system increases. In the case of 1.0% in a mass fraction of asphaltenes, the limits of each region and the mass change are affected. Remembering that for a concentration of 1.0% of asphaltenes, the aggregate size presents greater variations than at 0.1%, this parameter is correlated with the profiles obtained. The mass gained in OC for the three systems increases in the order: *p*-xylene < *m*-xylene < *o*-xylene. This result indicates that the larger the size of the asphaltene aggregate, the lower the interactions with O_2 because of a reduction in active sites of the asphaltene structure. Most of the asphaltenes in crude oil are polycyclic aromatic hydrocarbons capable of interacting with neighboring asphaltene molecules through several intermolecular forces, including London dispersion forces between aliphatic moieties, π-stacking of aromatic cores, hydrogen bonding between nitrogen-hydrogen and oxygen-hydrogen-containing functionalities, and acid/base interactions between carboxylic acids and pyridine rings.[45] That is, aromatic core-dominated interactions (π-stacking) drive asphaltene aggregation; however, it has been proven that heteroatom-based intermolecular forces also significantly affect the overall solubility and aggregation behavior.[4] These sites, in turn, are the main sites for oxygen chemisorption. The main difference is found in the mass gain during OC for a concentration of 10.0% in mass fraction of asphaltenes, which for the systems with *o*-, and *m*-xylene, the mass growth was higher in 7.2% and 6.5%, respectively, than *p*-xylene. This generates minor differences in the other regions since the reactivity of the systems depends on the structures formed during OC. In this sense, asphaltene model solution with a mass fraction of 10.0% in the *p*-xylene system completes the total decomposition 17 °C, and 11 °C after *o*-xylene, and *m*-xylene, respectively.

In this sense, depending on the solvent used, asphaltenes have greater or lesser interactions between them and the solvent. The reduction in OC as the aggregate size increases suggests a considerable increase in the interactions by alkyl-alkyl, hydrogen bonds, and acid/base.

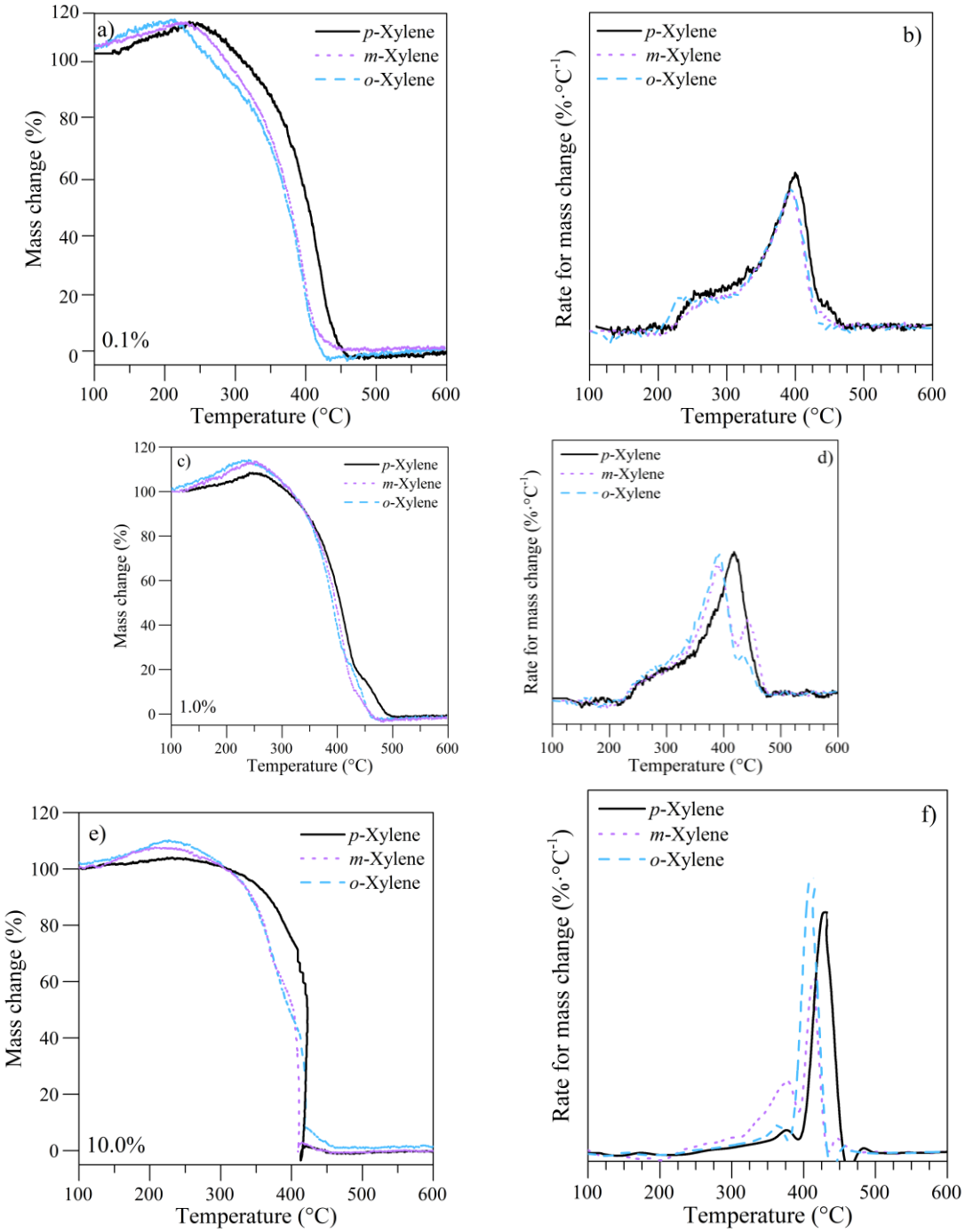

Figure 10. Mass percentage and rate for mass change for the thermo-oxidation of *n*-C_7 asphaltene model solutions in *o*-xylene, *m*-xylene, and *p*-xylene at different asphaltene concentrations of 0.1% (a-b), 1.0% (c-d), and 10.0% (e-f) at 6.0 MPa. Sample weight: 1 mg, heating rate: 10 °C·min^{-1}, and airflow: 80 mL·min^{-1}.

Due to the mass gained in OC, the thermal events DCO, FC, and SC change to a greater extent. First, the DCO region in systems with 10% in a mass fraction of asphaltenes ends at lower temperatures in *p*-xylene than *m*- and *o*-xylene due to the few oxygenated structures formed. Afterward, both FC and SC end up at higher temperatures. The main change is observed for the SC region, where the profiles for the model solutions of asphaltene with *m*- and *o*-xylene present a small peak between 400 and 500 °C, while in *p*-xylene, this is the predominant peak of the curve. Finally, a greater change is observed between the three curves for a concentration of 10.0% in mass fraction (panels e and f).

Furthermore, in previous work,[10] it was demonstrated that the size of the cluster of asphaltenes directly influences the rate of mass loss during FC and SC.[10] Asphaltenes with high *Lc* tend to present a violent exothermic reaction, resulting from the dealkylation of the structure.[9] According to the thermograms, all the systems offer a controlled loss of their mass, given that in all cases, the size of the added system is greater than those evaluated in previous works.

Kinetic analysis. Previous sections corroborated that the thermo-oxidation of asphaltene aggregates occurs throughout many competing complex reactions. The thermal profiles were described mathematically under four Gaussians, representing OC, DCO, FC, and SC. Kinetic fitting was successfully done by assuming a first-order kinetic model, i.e., n=1, obtaining $R^2 > 0.99$ for all cases.[49] The estimated effective activation energy of each thermal event for the different systems evaluated at 6.0 MPa are reported in Figure 11a-c.

As a first instance, it is observed that the effective activation energy is affected by the asphaltene aggregation state. Panel a shows the results for asphaltene aggregates formed with a content of 0.1% in mass fraction of *n*-C_7 asphaltenes. The values for OC region are similar in all cases following the incremental order: *o*-xylene < *m*-xylene < *p*-xylene. This behavior suggests that as the size of the asphaltene aggregate increases, the structure requires more energy for the chemical anchoring of oxygen. Notwithstanding, the difference between each system does not change greatly, as in the case of DCO, where the difference of E_α between the systems is much larger and follows the opposite order of OC. The different final structures can explain this at the end of OC in each system. Apparently, in the asphaltene aggregation state in *p*-xylene, less reactive structures are formed than in *m*- and *o*-xylene, so the value of E_α is much lower than the rest of the systems. Then, during the first combustion zone, E_α increases for all systems, meanwhile in SC is reduced in *o*-xylene. These results agree with the thermogravimetric profiles, where for the *p*-xylene aggregation state, the mass to decompose in SC is greater than for the rest of the systems. When the asphaltene concentration in the systems increases to 1.0% in mass fraction, there are similar trends to the previous systems. This is because the aggregate sizes do not differ much from each other. However, some important changes occur. The first is that the activation energy increases for OC in all systems, while DCO decreases for all systems, except for *p*-xylene. The latter is because, in this state of aggregation, all systems begin to lose reactivity since there is less oxygen chemisorption. Therefore the structures predominate their decomposition into FC and SC. That is the reason for these last two regions present values of E_α slightly higher than by 0.1%:

Something crucial for the systems with 0.1% and 1.0% of a mass fraction because OC is the most thermodynamically favorable event since lower E_α is always obtained.

Finally, panel c shows the results for the model solutions with 10.0% in mass fraction of asphaltenes. It is observed that the values for OC increased compared to the other two concentrations for all model solutions, confirming once again that in the larger aggregate complexes, the spontaneity of the asphaltene-oxygen interactions is decreased. Interestingly, in DCO, the value of E_α compared to OC, for *p*-xylene decreases, and in systems formed with *m*- and *o*-xylene, E_α remains almost constant.

In the case of FC, all systems increased the E_α since for these systems, in this region, there is still a high amount of mass for decomposing. The order increased as follows: *p*-xylene < *m*-xylene < *o*-xylene. *o*-Xylene presents the highest values because this model solution decomposes higher during this zone, whereas in SC, it decreases its value, while the other three systems behave differently. For all cases, it was obtained that the asphaltene aggregation state modifies the activation energy in each region, obtaining a global negative effect as the asphaltene size increases due to the increase in energy expenditure at higher temperatures.

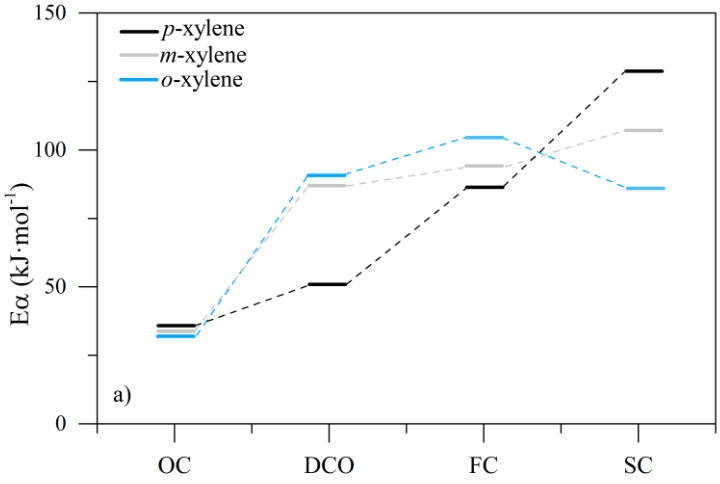

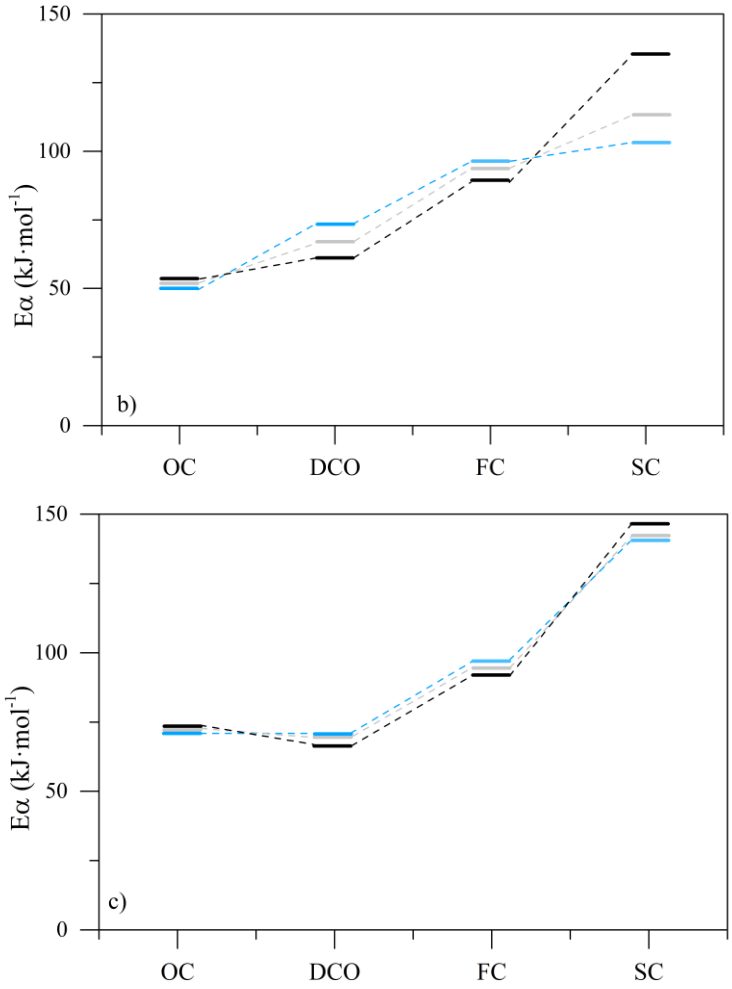

Figure 11. Estimated effective activation energy for the thermo-oxidation aggregates of *n*-C_7 asphaltenes with concentrations of a) 0.1%, b) 1.0%, and c) 10.0% in mass fraction, discretized in different thermal events named oxygen chemisorption (OC), desorption/decomposition of chemisorbed oxygen (DCO), first combustion (FC) and second combustion (SC) at 6.0 MPa.

Conclusions.

This work was done with the aim of understanding for the first time the thermo-oxidative behavior at high pressure of different asphaltene model solutions varying states of aggregation. As the first instance, the viscosity increases as the size of the asphaltene aggregate increases, and in turn, the viscosity increases as the asphaltene concentration in the model solution rise. For both low and high asphaltene concentrations, μ_r increases in the order *o*-xylene < *m*-xylene < *p*-xylene. MD simulations were carried out to understand why the location of the methyl substituent in the xylene structure modifies the rheological behavior from understanding the changes of the aggregation states. The RDF curves indicate a strong difference in the internal structure of the asphaltenes dissolved in each xylene isomer, obtaining that the asphaltene molecules are more structured (RDF peak of high intensity) for *p*-xylene than the other two xylene isomers. Hence, the asphaltene molecules tend to be more aggregated in *p*-xylene. This was corroborated by the analysis of the aggregate size, the asphaltene-asphaltene, and asphaltene-xylene interaction energies, which showed that the asphaltenes are less aggregated in *o*-xylene, followed by *m*-xylene and *p*-xylene in that order. RDF between the asphaltenes and the carbon atoms of the methyl substituents demonstrated that the methyl substituents are oriented towards asphaltenes, in the case of *o*-xylene, increasing the number of near and far neighbors, compared to the other two cases. Therefore, a strong entropic volume effect is determined as a consequence of the location of the $–CH_3$, which increases the asphaltene-xylene interaction energies impacting the aggregation and rheological behavior.

The second section includes the high-pressure thermogravimetric analysis to assess the thermo-oxidative behavior of asphaltene aggregates. In the first set of thermogravimetric experiments, the concentration of asphaltenes varied between 0.1% and 10% in mass fraction to evaluate its effect on the reactivity of the model solutions, using *p*-xylene as a reference solvent. The results showed that the oxygen chemisorption decreased as the asphaltene concentration increased in the system, and therefore the reactivity was reduced. Finally, three aromatic solvents (*p*-xylene, *m*-xylene, and *o*-xylene) of similar solubility parameters but with different chemical structures

were chosen so the effect of the location of a methyl group on the solvent molecule on thermo-oxidation reactions can be analyzed. There is no significant change in the thermogravimetric profiles for a concentration of 0.1% by a mass fraction in the different solvents used. However, with increasing the concentration to 1.0 and 10.0%, the mass gained by oxygen chemisorption increased in the order: *o*-xylene <*m*-xylene <*p*-xylene <toluene. This result indicates that the larger the size of the asphaltene aggregate, the lower the interactions with O_2 because of a reduction in active sites of the asphaltene structure.

References

1. Medina, O. E.; Olmos, C.; Lopera, S. H.; Cortés, F. B.; Franco, C. A., Nanotechnology applied to thermal enhanced oil recovery processes: a review. *Energies* **2019,** 12, (24), 4671.
2. Dabbous, M. K.; Fulton, P. F., Low-temperature-oxidation reaction kinetics and effects on the in-situ combustion process. *Society of Petroleum Engineers Journal* **1974,** 14, (03), 253-262.
3. Kök, M. V.; Karacan, Ö.; Pamir, R., Kinetic analysis of oxidation behavior of crude oil SARA constituents. *Energy & Fuels* **1998,** 12, (3), 580-588.
4. Acevedo, S.; Castillo, J.; Vargas, V.; Castro, A.; Delgado, O. Z.; Ariza, C. A. F.; Cotés, F. B.; Bouyssiere, B., Suppression of Phase Separation as a Hypothesis to Account for Nuclei or Nanoaggregate Formation by Asphaltenes in Toluene. *Energy & Fuels* **2018**.
5. Liu, D.; Hou, J.; Luan, H.; Pan, J.; Song, Q.; Zheng, R., Coke yield prediction model for pyrolysis and oxidation processes of low-asphaltene heavy oil. *Energy & Fuels* **2019,** 33, (7), 6205-6214.
6. Amrollahi Biyouki, A.; Hosseinpour, N.; Nassar, N. N., Pyrolysis and Oxidation of Asphaltene-Born Coke-like Residue Formed onto in Situ Prepared NiO Nanoparticles toward Advanced in Situ Combustion Enhanced Oil Recovery Processes. *Energy & fuels* **2018,** 32, (4), 5033-5044.
7. Zhao, S.; Pu, W.; Yuan, C.; Peng, X.; Zhang, J.; Wang, L.; Emelianov, D. A., Thermal behavior and kinetic triplets of heavy crude oil and its SARA fractions during combustion by high-pressure differential scanning calorimetry. *Energy & fuels* **2019,** 33, (4), 3176-3186.
8. Yuan, C.; Varfolomeev, M. A.; Emelianov, D. A.; Eskin, A. A.; Nagrimanov, R. N.; Kok, M. V.; Afanasiev, I. S.; Fedorchenko, G. D.; Kopylova, E. V., Oxidation behavior of light crude oil and its SARA fractions characterized by TG and DSC techniques: differences and connections. *Energy & fuels* **2018,** 32, (1), 801-808.
9. Medina, O. E.; Gallego, J.; Rodríguez, E.; Franco, C. A.; Cortés, F. B., Effect of pressure on the oxidation kinetics of Asphaltenes. *Energy & Fuels* **2019,** 33, (11), 10734-10744.
10. Medina, O. E.; Gallego, J.; Nassar, N. N.; Acevedo, S. A.; Cortés, F. B.; Franco, C. A., Thermo-Oxidative Decomposition Behaviors of Different Sources of n-C7 Asphaltenes at High-Pressure Conditions. *Energy & Fuels* **2020**.
11. Moncayo-Riascos, I.; Taborda, E.; Hoyos, B. A.; Franco, C. A.; Cortés, F. B., Theoretical-experimental evaluation of rheological behavior of asphaltene solutions in toluene and p-xylene: Effect of the additional methyl group. *Journal of Molecular Liquids* **2020,** 303, 112664.
12. Tanaka, R.; Hunt, J. E.; Winans, R. E.; Thiyagarajan, P.; Sato, S.; Takanohashi, T., Aggregates structure analysis of petroleum asphaltenes with small-angle neutron scattering. *Energy & fuels* **2003,** 17, (1), 127-134.
13. Lee, H.; Lee, Y.-K., Effects of the asphaltene structure and the tetralin/heptane solvent ratio on the size and shape of asphaltene aggregates. *Physical Chemistry Chemical Physics* **2017,** 19, (21), 13931-13940.
14. Larichev, Y. V.; Nartova, A.; Martyanov, O., The influence of different organic solvents on the size and shape of asphaltene aggregates studied via small-angle X-ray scattering and scanning tunneling microscopy. *Adsorption Science & Technology* **2016,** 34, (2-3), 244-257.
15. Hu, D.; Gu, X.; Cui, B.; Pei, J.; Zhang, Q., Modeling the oxidative aging kinetics and pathways of asphalt: A ReaxFF molecular dynamics study. *Energy & Fuels* **2020,** 34, (3), 3601-3613.
16. Lan, T.; Zeng, H.; Tang, T., Understanding adsorption of violanthrone-79 as a model asphaltene compound on quartz surface using molecular dynamics simulations. *The Journal of Physical Chemistry C* **2018,** 122, (50), 28787-28796.
17. Law, J. C.; Headen, T. F.; Jiménez-Serratos, G.; Boek, E. S.; Murgich, J.; Müller, E. A., Catalogue of Plausible Molecular Models for the Molecular Dynamics of Asphaltenes and Resins Obtained from Quantitative Molecular Representation. *Energy & Fuels* **2019,** 33, (10), 9779-9795.
18. Hosseini-Dastgerdi, Z.; Tabatabaei-Nejad, S.; Khodapanah, E.; Sahraei, E., A comprehensive study on mechanism of formation and techniques to diagnose asphaltene structure; molecular and aggregates: a review. *Asia-Pacific Journal of Chemical Engineering* **2015,** 10, (1), 1-14.
19. Barre, L.; Espinat, D.; Rosenberg, E.; Scarsella, M., Colloidal structure of heavy crudes and asphaltene soltutions. *Revue de l'Institut Français du Pétrole* **1997,** 52, (2), 161-175.

20. Medina, O. E.; Gallego, J.; Acevedo, S.; Riazi, M.; Ocampo-Pérez, R.; Cortés, F. B.; Franco, C. A., Catalytic Conversion of n-C7 Asphaltenes and Resins II into Hydrogen Using CeO2-Based Nanocatalysts. *Nanomaterials* **2021,** 11, (5), 1301.
21. Tanaka, R.; Sato, E.; Hunt, J. E.; Winans, R. E.; Sato, S.; Takanohashi, T., Characterization of asphaltene aggregates using X-ray diffraction and small-angle X-ray scattering. *Energy & fuels* **2004,** 18, (4), 1118-1125.
22. Eyssautier, J.; Frot, D.; Barré, L., Structure and dynamic properties of colloidal asphaltene aggregates. *Langmuir* **2012,** 28, (33), 11997-12004.
23. Larichev, Y. V.; Martyanov, O., The dynamics of asphaltene aggregates in heavy crude oils on a nanometer scale studied via small-angle X-ray scattering in situ. *Journal of Petroleum Science and Engineering* **2018,** 165, 575-580.
24. Petoukhov, M. V.; Franke, D.; Shkumatov, A. V.; Tria, G.; Kikhney, A. G.; Gajda, M.; Gorba, C.; Mertens, H. D.; Konarev, P. V.; Svergun, D. I., New developments in the ATSAS program package for small-angle scattering data analysis. *Journal of applied crystallography* **2012,** 45, (2), 342-350.
25. Gimzewski, E., An accurate and compact high-pressure thermogravimetric analyser. *Journal of thermal analysis* **1991,** 37, (6), 1251-1260.
26. Medina, O. E.; Gallego, J.; Rodriguez, E.; Franco, C. A.; Cortés, F. B., Effect of Pressure on the Oxidation Kinetics of Asphaltenes. *Energy & Fuels* **2019**.
27. Xu, Z.; Wang, Y.; Cao, J.; Chai, J.; Cao, C.; Si, Z.; Li, Y., Adhesion between asphalt molecules and acid aggregates under extreme temperature: A ReaxFF reactive molecular dynamics study. *Construction and Building Materials* **2021,** 285, 122882.
28. Headen, T.; Boek, E.; Jackson, G.; Totton, T.; Müller, E., Simulation of asphaltene aggregation through molecular dynamics: Insights and limitations. *Energy & Fuels* **2017,** 31, (2), 1108-1125.
29. Jorgensen, W.; Maxwell, D.; Tirado-Rives, J., Optimized potential for liquid simulations. *J. Am. Chem. Soc* **1996,** 118, 11225-11236.
30. Jorgensen, W. L.; Maxwell, D. S.; Tirado-Rives, J., Development and testing of the OPLS all-atom force field on conformational energetics and properties of organic liquids. *Journal of the American Chemical Society* **1996,** 118, (45), 11225-11236.
31. Watkins, E. K.; Jorgensen, W. L., Perfluoroalkanes: Conformational analysis and liquid-state properties from ab initio and Monte Carlo calculations. *The Journal of Physical Chemistry A* **2001,** 105, (16), 4118-4125.
32. Plimpton, S., Fast parallel algorithms for short-range molecular dynamics. *Journal of computational physics* **1995,** 117, (1), 1-19.
33. Humphrey, W.; Dalke, A.; Schulten, K., VMD: visual molecular dynamics. *Journal of molecular graphics* **1996,** 14, (1), 33-38.
34. Senneca, O.; Vorobiev, N.; Wütscher, A.; Cerciello, F.; Heuer, S.; Wedler, C.; Span, R.; Schiemann, M.; Muhler, M.; Scherer, V., Assessment of combustion rates of coal chars for oxy-combustion applications. *Fuel* **2019,** 238, 173-185.
35. Niksa, S.; Liu, G.-S.; Hurt, R. H., Coal conversion submodels for design applications at elevated pressures. Part I. devolatilization and char oxidation. *Progress in Energy and Combustion Science* **2003,** 29, (5), 425-477.
36. Liu, G.-S.; Niksa, S., Coal conversion submodels for design applications at elevated pressures. Part II. Char gasification. *Progress in energy and combustion science* **2004,** 30, (6), 679-717.
37. Yen, T. F.; Erdman, J. G.; Pollack, S. S., Investigation of the structure of petroleum asphaltenes by X-ray diffraction. *Analytical chemistry* **1961,** 33, (11), 1587-1594.
38. AlHumaidan, F. S.; Hauser, A.; Rana, M. S.; Lababidi, H. M., NMR Characterization of Asphaltene Derived from Residual Oils and Their Thermal Decomposition. *Energy & Fuels* **2017,** 31, (4), 3812-3820.
39. Vukovic, J. P.; Novak, P.; Jednacak, T., NMR Spectroscopy as a Tool for Studying Asphaltene Composition. *Croatica Chemica Acta* **2019,** 92, (3), 1G-1G.
40. Retcofsky, H.; Schweighardt, F.; Hough, M., Determination of aromaticities of coal derivatives by nuclear magnetic resonance spectrometry and the Brown-Ladner equation. *Analytical Chemistry* **1977,** 49, (4), 585-588.
41. Pierre, C.; Barré, L.; Pina, A.; Moan, M., Composition and heavy oil rheology. *Oil & Gas Science and Technology* **2004,** 59, (5), 489-501.
42. Taborda, E. A.; Alvarado, V.; Franco, C. A.; Cortés, F. B., Rheological demonstration of alteration in the heavy crude oil fluid structure upon addition of nanoparticles. *Fuel* **2017,** 189, 322-333.
43. Ramírez, L.; Moncayo-Riascos, I.; Cortés, F. B.; Franco, C. A.; Ribadeneira, R., Molecular Dynamics Study of the Aggregation Behavior of Polycyclic Aromatic Hydrocarbon Molecules in n-Heptane–Toluene Mixtures: Assessing the Heteroatom Content Effect. *Energy & Fuels* **2021,** 35, (4), 3119-3129.
44. Moncayo-Riascos, I.; Taborda, E.; Hoyos, B. A.; Franco, C. A.; Cortés, F. B., Effect of resin/asphaltene ratio on the rheological behavior of asphaltene solutions in a de-asphalted oil and p-xylene: A theoretical–experimental approach. *Journal of Molecular Liquids* **2020,** 315, 113754.

45. Johansson, B.; Friman, R.; Hakanpää-Laitinen, H.; Rosenholm, J. B., Solubility and interaction parameters as references for solution properties II: Precipitation and aggregation of asphaltene in organic solvents. *Advances in colloid and interface science* **2009,** 147, 132-143.
46. Pal, R., A new model for the viscosity of asphaltene solutions. *The Canadian Journal of Chemical Engineering* **2015,** 93, (4), 747-755.
47. Kuakpetoon, D.; Wang, Y.-J., Structural characteristics and physicochemical properties of oxidized corn starches varying in amylose content. *Carbohydrate Research* **2006,** 341, (11), 1896-1915.
48. Andreatta, G.; Bostrom, N.; Mullins, O. C., High-Q ultrasonic determination of the critical nanoaggregate concentration of asphaltenes and the critical micelle concentration of standard surfactants. *Langmuir* **2005,** 21, (7), 2728-2736.
49. Medina Erao, O. E.; Gallego, J.; Olmos, C. M.; Chen, X.; Cortés, F. B.; Franco, C. A., Effect of Multifunctional Nanocatalysts on n-C7 Asphaltene Adsorption and Subsequent Oxidation under High Pressure Conditions. *Energy & Fuels* **2020**.

Appendix A.

Table 1. Average molecular structure parameter of *n*-C_7 asphaltenes, obtained through the chemical elemental analysis and ^{1}H-NMR spectra

Parameter	Description	*n*-C_7 Asphaltenes
f_A	Aromaticity Factor	0.645
σ	Hydrogen periphery replacement rate in the aromatic ring system	0.093
H_{AU}/C_A	Condensation degree parameter of the aromatic ring system	0.388
H_T	Total hydrogen numbers	70.746
C_T	Total carbon numbers	74.102
C_A	Aromatic carbon numbers	47.788
C_S	Saturated carbon numbers	26.314
C_α	Carbon numbers on the α position of an aromatic ring	1.696
C_{ap}	Peripheral carbon in a fused aromatic ring	18.320
C_i	Internal carbon in a fused aromatic ring	29.468
R_{Ar}	Aromatic rings	15.734
R_t	Total rings	15.835
R_n	Naphthenic rings	0.101
n	Average alkyl chain length	15.956

Table 2. Thermogravimetric characteristics for the thermo-oxidation of *n*-C_7 asphaltene model solutions in toluene at different asphaltene concentrations of 0.1%, 1.0%, and 10.0% discretized in the different regions: *i*) oxygen chemisorption (OC) *ii*) decomposition of the chemisorbed oxygen (DCO) region, *iii*) first combustion (FC) region and *iv*) second combustion (SC) region at 6.0 MPa.

Asphaltene Concentration (% mass fraction)	OC Region		DCO Region		FC Region		SC Region	
	Temperature range (°C)	Mass gain (mass fraction in %)	Temperature range (°C)	Mass loss (mass fraction in %)	Temperature range (°C)	Mass loss (mass fraction in %)	Temperature range (°C)	Mass loss (mass fraction in %)
0.1	100-226	11.0	227-314	13.1	315-425	75.9	426-443	22.0
1.0	100-241	9.3	242-312	10.5	313-415	53.8	416-455	45.0
10.0	100-248	2.3	249-325	5.9	326-375	18.0	376-477	80.0

Table 3. Thermogravimetric characteristics for the thermo-oxidation of *n*-C_7 asphaltene model solutions in *o*-xylene, *m*-xylene, and *p*-xylene at different asphaltene concentrations of 0.1%, 1.0%, and 10.0% discretized in the different regions: *i*) oxygen chemisorption (OC) *ii*) decomposition of the chemisorbed oxygen (DCO) region, *iii*) first combustion (FC) region and *iv*) second combustion (SC) region at 6.0 MPa.

Solvent	Asphaltene Concentration (% mass fraction)	OC Region		DCO Region		FC Region		SC Region	
		Temperature range (°C)	Mass gain (mass fraction in %)	Temperature range (°C)	Mass loss (mass fraction in %)	Temperature range (°C)	Mass loss (mass fraction in %)	Temperature range (°C)	Mass loss (mass fraction in %)
o-xylene	0.1	100-228	12.9	229-317	18.1	318-399	80.5	400-440	14.3
	1.0	100-230	10.0	231-320	17.2	321-402	76.6	403-445	15.9
	10.0	100-215	9.5	216-330	11.6	331-409	48.9	410-450	47.0
m-xylene	0.1	100-227	12.7	228-315	15.9	316-412	77.3	413-442	19.5
	1.0	100-232	10.1	233-314	16.5	315-410	65.9	411-450	27.7
	10.0	100-218	8.8	219-328	10.2	329-394	49.4	395-456	47.5
p-xylene	0.1	100-226	11.0	227-314	13.1	315-425	75.9	426-443	22.0
	1.0	100-241	9.3	242-312	10.5	313-415	53.8	416-455	45.0
	10.0	100-248	2.3	249-325	5.9	326-375	18.0	376-477	80.0